Small-displacement soil-structure interaction for horizontally loaded piles in sand

S. P. H. Sørensen
COWI A/S, Denmark, spso@cowi.dk

A. H. Augustesen
COWI A/S, Denmark

ABSTRACT
Monopile foundations with diameters of 4 to 6 m are often employed for offshore wind turbines. The Winkler model approach, where the soil pressure acting against the pile wall is provided by uncoupled springs with stiffness provided by p-y curves, is traditionally employed in the design. However, the p-y curves currently recommended by Det Norske Veritas and the American Petroleum Institute are developed for slender piles with diameters up to approximately 2 m when considering piles in sand.
In the serviceability limit state, only small rotations of the monopiles are allowed. Hereby, the initial part of the p-y curves, is of high importance in the design of monopile foundations for offshore wind turbines.
The aim of the paper is to investigate the small-displacement stiffness of the soil-pile interaction for large-diameter stiff piles in sand subjected to lateral loading. A modified expression for the static part of the p-y curves is investigated in which the initial slope of the p-y curves depends on the depth below the soil surface, the pile diameter and Young's modulus of elasticity of the soil. Three-dimensional numerical analyses conducted by means of the commercial program FLAC^{3D} incorporating a Mohr-Coulomb failure criterion are the basis for the research.

Keywords: Piles, soil/structure interaction, p-y curve, numerical modelling, sand.

1 INTRODUCTION

The monopile foundation concept is often employed in the design of offshore wind turbines. Monopiles are welded steel pipe piles driven open-ended into the soil. In order to be able to sustain the large forces and moments, the outer pile diameter, D, is typically five to eight meters with an embedded pile length, L_p, in the range of 20 to 35 m. Hence, the slenderness ratio, L_p/D, is around five.

The American Petroleum Institute (ANSI/API, 2011) and Det Norske Veritas (DNV, 2014), recommend to employ the Winkler model approach in the design of monopiles, i.e. the pile is considered as a beam on an elastic foundation. The elastic foundation consists of a discrete number of springs with stiffness determined by means of *p-y* curves. *p-y* curves describe the soil resistance, *p*, acting against the pile wall as a function of the lateral pile deflection, *y*.

For piles in sand, ANSI/API (2011) and DNV (2014) recommend a *p-y* curve formulation, which has been validated for slender piles with diameters up to approximately 2 m, cf. Cox et al. (1974) and Murchison and O'Neill (1984). The formulation has, however, not been validated for piles with diameters of five to eight meter and slenderness ratios around five. Hereby, the influence of pile properties such as the pile diameter and the pile slenderness ratio on the soil response still need to be investigated.

In the serviceability limit state, only small rotations of the monopiles are allowed. Further, strict demands are set to the total stiffness of the foundation in order to avoid resonance with the rotor and blade passing frequencies and with the wind and wave loading. Hereby, the small-displacement stiffness,

e.g. the first part of the *p-y* curves, is of high importance in the design of monopile foundations for offshore wind turbines.

In the present paper, the *p-y* curve formulation recommended by ANSI/API (2011) and DNV (2014) is re-evaluated for static loading conditions. The main focus is on the first part of the *p-y* curves. In the design of offshore wind turbine foundations, the cyclic behaviour is of high interest due to the cyclic behaviour of wind and wave loads. However, the trend of the first part of the *p-y* curves is expected to be similar for static and cyclic loading. According to Kramer (1996) the backbone curve of a soil can be described by two parameters: the initial (low-strain) stiffness and the (high-strain) shear strength. Similarly, it is assumed that the soil-structure interaction similarly can be described by an initial slope, *dp*/*dy*, and an ultimate resistance. An expression of the slope of the *p-y* curves at small displacements, but not the true initial tangent stiffness, is proposed aiming at accurate predictions of the pile behaviour when the pile is exposed to serviceability limit state (SLS) loads and lower bound system frequency analyses. The expression is determined based on a numerical study. The effect on the pile behaviour by incorporating the modified expression for the initial slope of the *p-y* curves in a Winkler model is illustrated for a monopile foundation situated at Horns Rev, Denmark.

2 *p-y* CURVE FORMULATION

ANSI/API (2011) and DNV (2014) recommend the *p-y* curve formulation given in equation (1) for piles located in sand.

$$p(y) = Ap_u \tanh\left(\frac{kx}{Ap_u}y\right) \tag{1}$$

p_u is the ultimate soil resistance, k is the initial modulus of subgrade reaction and x is the depth below the soil surface. A is a dimensionless factor depending on the loading scenario, i.e. static or cyclic:

$$A = \min\begin{Bmatrix} 3.0 - 0.8\frac{x}{D} \geq 0.9 & \text{, Static loading} \\ 0.9 & \text{, Cyclic loading} \end{Bmatrix} \tag{2}$$

The ultimate soil resistance can in accordance with Bogard and Matlock (1980) be estimated as:

$$p_u = \min\begin{Bmatrix} (C_1 x + C_2)\gamma' x \\ C_3 D \gamma' x \end{Bmatrix} \tag{3}$$

C_1, C_2 and C_3 are dimensionless factors varying with the internal friction angle, φ. k depends on the relative density/internal friction angle of the soil. The true initial slope of the *p-y* curves denoted E^*_{py} is thereby:

$$E^*_{py} = \left.\frac{dp}{dy}\right|_{y=0} = kx \tag{4}$$

Hence, E^*_{py} is considered explicitly to be independent of the pile properties, e.g. the pile diameter, D, the slenderness ratio, L_p/D, and the pile bending stiffness, E_pI_p. E^*_{py} varies linearly with depth below the soil surface and the initial modulus of subgrade reaction, k.

Several authors have investigated the influence of the pile diameter on E^*_{py} with contradictory conclusions. Terzaghi (1955), Ashford and Juirnarongrit (2003) and Fan and Long (2005) conclude that the pile diameter has no significant effect on the initial slope of the *p-y* curves. In contrast, Carter (1984) and Ling (1988) propose a linear dependency between pile diameter and initial stiffness.

Based on numerical investigations and a linear variation of E^*_{py} with depth as given in equation (4), Lesny and Wiemann (2006) conclude that the stiffness is overestimated for large depths. Instead, they propose a nonlinear variation of E^*_{py} with depth, i.e. E^*_{py} is proportional with $x^{0.6}$.

Based on theoretical considerations concerning changes in shear modulus as a function of shear strain and a nonlinear increase with depth, Kallehave et al. (2012) suggest a modified expression for the initial slope of the *p-y* curves in sand. They aim at improving the approximation of the natural frequency for offshore wind turbines supported by

monopile foundations. An expression in which the initial slope of the *p-y* curves is proportional to the depth raised to the power of *m* and to the pile diameter raised to the power of *n* is suggested. The values of the dimensionless factors *m* and *n* are site specific. In a benchmark study of full-scale measurements from three wind turbines in the Walney offshore wind farm, values of $m = 0.6$ and $n = 0.5$ are proposed.

Kirsch et al. (2104) has suggested a modification to the initial modulus of subgrade reaction, *k*, in which it is attempted to account for large-diameter effects and the small-strain stiffness.

Based on centrifuge tests on piles with slenderness ratios of 2 to 10, Leth (2013) concludes that the small-displacement stiffness (evaluated at a normalized pile head displacement of 1%) of the *p-y* curves is proportional to the depth below soil surface raised to a power of 0.5 and to the pile diameter raised to the power of 0.6. Hence, while the considerations of Kallehave et al. (2012) aim at predicting the low-strain response, Leth (2013) aims at modelling the pile response corresponding to the serviceability limit state (SLS) loads.

The pile-soil interaction and pile response are affected by the flexibility of the pile. The slenderness ratio for monopiles for modern offshore wind turbines is significantly lower than the slenderness ratio for the piles tested at Mustang Island. Therefore, monopiles used for offshore wind turbine foundations exhibit a rather stiff behaviour in contrast to the rather flexible piles for which the currently recommended *p-y* formulation has been validated.

In conclusion, the *p-y* curve formulation currently recommended by ANSI/API (2011) and DNV (2014) is at first sight not well suited for the design of monopile foundations for offshore wind turbines. Knowledge is especially needed regarding the *p-y* curves at small displacements.

3 NUMERICAL MODELLING

3.1 Establishing the numerical model

A numerical model has been constructed in the commercial program *FLAC*^{3D} (FLAC^{3D} 3.1, 2006), with the objective of determining the behaviour of monopiles exposed to static lateral loading.

Since, the model is symmetric around a vertical plane parallel with the lateral loading direction only half of the pile and surrounding soil is modelled. The pile and the soil are divided into zones consisting of five 4-noded constant strain-rate sub-elements of tetrahedral shape (approximately 20000 zones have been employed). An outer diameter of 40*D* is used whereas the bottom boundary is placed 15 m below the pile toe. This ensures that the model boundaries do not influences the results. Standard boundary conditions have been applied to the model boundary.

For practical reasons the pile is modelled as a solid pile. Therefore, the Young's modulus of elasticity and the density of the solid pile are scaled to ensure that the bending stiffness and the weight including soil are identical to the properties of a tubular pile. The plug ratio is assumed equal to unity. The shear stiffness, A_pG_p, is not scaled correctly, which is of minor importance since bending is governing in the design. Analyses, not presented here, show that the difference in the maximum deflections at the seabed for a pile with $L_p/D = 5$ is less than 2 % when comparing the results based on the solid pile model with the results obtained by means of a tubular pile model.

The Mohr-Coulomb material model is employed for the sand. The reason for using a simple model is that the soil parameters employed in the model can be determined from few experimental tests. Further, it is convenient to have few model parameters in a parametric study. Hence, it seems naturally to incorporate a material model with only one stiffness parameter. The disadvantage with respect to the chosen material model is that the model does not take into account the stress and strain dependency of soil stiffness. However, Achmus et al. (2009), Chik et al. (2009) and Kim and Jeong (2011) have suc-

cessfully modelled horizontally loaded piles by employing the Mohr-Coulomb material model for the soil. The interface between the pile and the soil is modelled by means of a linear Coulomb shear strength criterion allowing gapping and slipping between the pile and the soil.

A displacement-controlled horizontal loading is applied as a velocity to the centre nodes of the pile head. Hereby, a number of steps are prescribed in order to reach the desired pile deflection. To ensure a quasi-static behaviour of the pile-soil system, the velocity of the pile is set to 10^{-6} ms^{-1}.

Damping is introduced since *FLAC*^{3D} is a dynamic, explicit finite difference solver.
The numerical simulations are executed in stages. First, the initial stresses in the soil are generated using a K_0-procedure. Secondly, an equilibrium state is established for the pile and the soil in which the soil properties are employed for the pile material. At this stage, the interface between the soil and the pile is assumed smooth. Thirdly, a new equilibrium state is calculated in which the pile and the interface are given the correct properties. After reaching equilibrium, the horizontal load is applied as described.

3.2 Validation

The numerical model has been validated against 23 laboratory tests conducted in a so-called pressure tank, cf. Sørensen et al. (2015). The laboratory tests were carried out on piles with diameters of 40-100 mm and embedded pile lengths of 200-500 mm embedded in dense to very dense fine sand. The piles were exposed to lateral loading.

Results from one test (L_p/D = 5 and overburden pressure of P_0 = 100 kPa and D = 100 mm) as well as load-settlement curves established by means of the FLAC^{3D} model are shown in Figure 1. A reasonable concordance between the numerical simulations and the test results has been found for y/D less than 0.2.

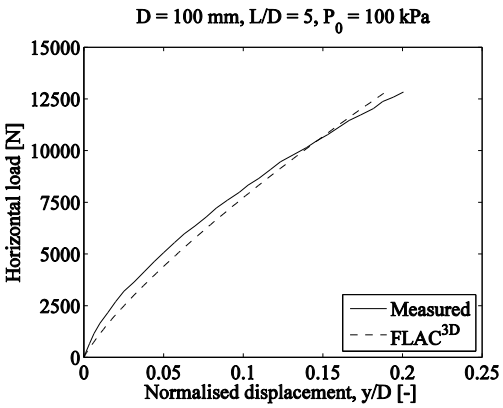

Figure 1 Comparison of numerical simulations and laboratory tests.

3.3 Pile and soil properties

Steel piles with pile diameters of D = 1-7 m and length of L_p = 20 m have been studied. Hence, the slenderness ratio, L_p/D, varies between 3 and 20. For practical purposes the pile wall thickness, *wt*, is assumed constant and equal to 0.05 m. For D = 1 m flexible pile behaviour is expected while a rather rigid pile behaviour is expected for D = 7 m.

According to Klinkvort et al. (2010), the location of the force resultant, *e*, with respect to the embedment length, L_p, influences the shape of the *p-y* curves. Normally, e/L_p is in the interval of 0.5 to 2.0 for the design load of monopiles for offshore wind turbines. In this study, e/L_p = [0.50; 0.75; 1.00; 1.50; 2.00] have been applied.

A Young's modulus of elasticity, E_p, a Poisson's ratio, ν, and a unit weight, γ, of 210 GPa, 0.3 and 77 kNm^{-3}, respectively, have been assumed for the steel material. A homogeneous soil is employed. The internal friction angle, φ, of the sand has been varied between 30-43°. The wall friction angle, δ, between the soil and the pile is as proposed by Brinkgreve and Swolfs (2007) set to:

$$\delta = \text{atan}\left(\frac{2\tan(\varphi)}{3}\right) \quad (5)$$

Hereby, the wall friction angle takes values from 21° to 32°. The dilatancy angle, ψ, of the soil material is given in equation (8) (Brinkgreve and Swolfs, 2007):

$$\psi = \varphi - 30 \quad (6)$$

Young's modulus of elasticity for the soil has been varied in the range 21 to 93 MPa. Generally, the stiffness of sand is stress dependent. However, in order to decouple the influence of soil stiffness and depth below soil surface on E^*_{py}, the Young's modulus of elasticity for the soil, E_s, has been assumed constant with depth in the parametric study of parameters influencing the small-displacement stiffness of the *p-y* curves.

4 RESULTS

4.1 Effects of L_p/D, E_pI_p, e/L_p and soil properties on the pile response

Figure 2 and Figure 3 present pile deflections and bending moment distributions for piles with D = 1-7 m and φ = 37°, respectively. For D = 7 m the pile behaves very stiff. In contrast, the pile with D = 1 m behaves flexible. The depth to the point of zero deflection increases for increasing pile diameter. Furthermore, the depth to the maximum bending moment increases for increasing pile diameter. Since the length has been kept constant at 20 m, the slenderness ratio, L_p/D, varies as the pile diameter is varied. Hereby, it can be concluded that the slenderness ratio has a significant effect on the pile behaviour.

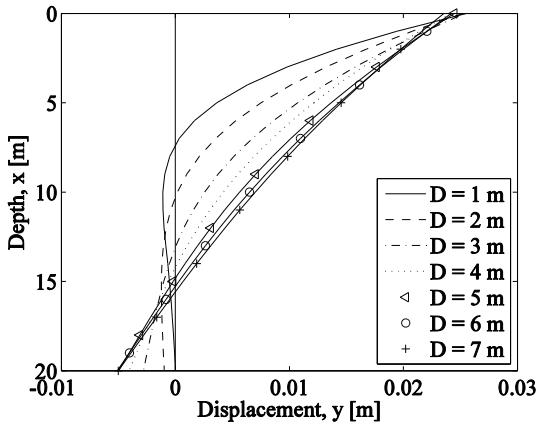

Figure 2 Pile deflection along the pile for φ_{tr} = 37°, E_s = 59 MPa, wt = 0.05 m, L_p = 20 m and e/L_p = 0.75.

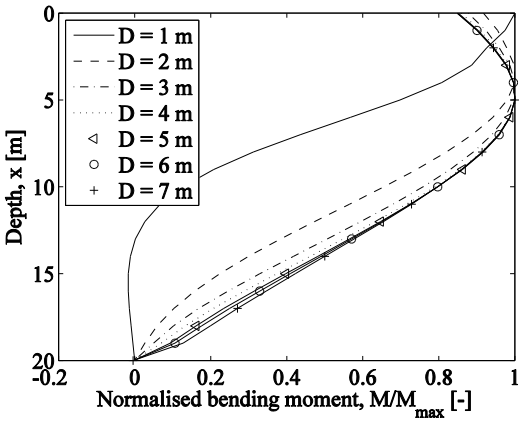

Figure 3 Distribution of bending moment. φ_{tr} = 37°, E_s = 59 MPa, wt = 0.05 m, L_p = 20 m and e/L_p = 0.75.

Figure 4 illustrates the variation of the small-displacement stiffness of the *p-y* curves, E^*_{py} with pile diameter, D, and depth below soil surface. In practice E^*_{py} has been estimated as the secant stiffness for a pile deflection of 1.5 mm. Hence, the small displacement stiffness is investigated and not the true initial stiffness. A non-linear increase of $E_{py}{}^*$ can be observed for increasing depths, which is in contrast to the linear dependency proposed by ANSI/API (2011) and DNV (2014). Further, E^*_{py} is found to increase for increasing pile diameter primarily due to differences in pile deflection behaviour going from flexible for small pile diameters and high slenderness ratios to stiff body rotations for large diameters and low slenderness ratios. In contrast, ANSI/API (2011) and DNV (2014) propose that E^*_{py} is independent of the pile diameter. The rotation of the pile causes discontinuities in the values of E^*_{py} at depths between approximately 8-17 m as the point of rotation changes with the size of loading. Therefore, values of E^*_{py} at these depths are left out in the following figures.

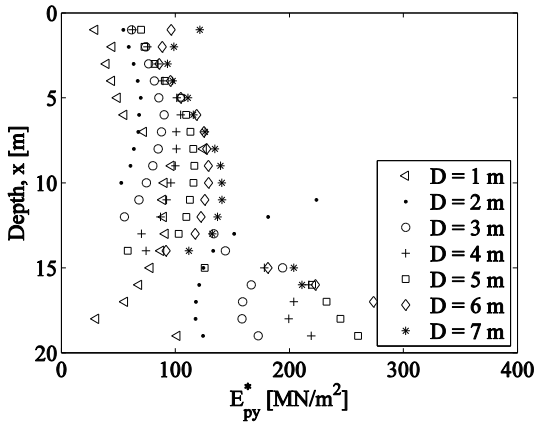

Figure 4 Variation of small-displacement stiffness, E^*_{py}, with depth for φ_{tr} = 37°, E_s = 59 MPa, wt = 0.05 m, L_p = 20 m and e/L_p = 0.75.

Figure 5, Figure 6 and Figure 7 illustrate the variation of the small-displacement stiffness of the *p-y* curves, E^*_{py} with friction angle, φ, Young's modulus of elasticity for the soil, E_s, and loading eccentricity, e/L_p, respectively. According to Figure 5, E^*_{py} is insignificantly influenced by the internal friction angle. Furthermore, Figure 6 indicates that E^*_{py} increases with increasing values of Young's modulus of the soil, E_s. However, ANSI/API (2011) and DNV (2014) suggest that E^*_{py} is independent on the Young's modulus of elasticity of the soil and instead dependent on the internal friction angle. However, it should be noted that Young's modulus of elasticity of the soil and the internal friction angle are interrelated via the relative density of the sand. Figure 7 indicates that E^*_{py} is independent of the loading eccentricity for e/L_p = 0.5-2.0.

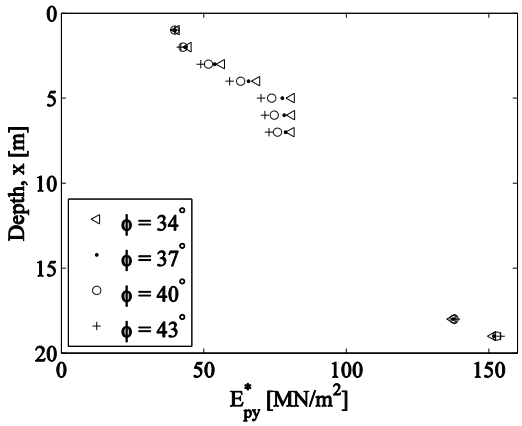

Figure 5 Variation of small-displacement stiffness, E^*_{py}, with depth for varying internal friction angles D = 5 m, E_s = 59 MPa, wt = 0.05 m, L_p = 20 m and e/L_p = 0.75.

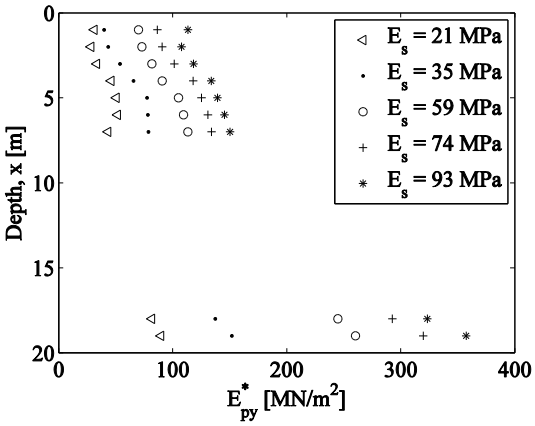

Figure 6 Variation of small, displacement stiffness, E^*_{py}, with depth for varying values of E_s. φ_{tr} = 37°, E_s = 59 MPa, wt = 0.05 m, L_p = 20 m and e/L_p = 0.75.

Figure 8 presents the influence of bending stiffness, E_pI_p, on the *p-y* curves. It can be concluded that E_pI_p does not influence the *p-y* curves. This is in agreement with Fan and Long (2005), but in contrast to Ashour and Norris (2000).

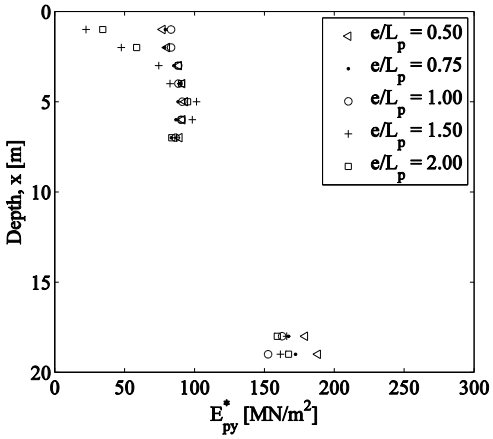

*Figure 7 Variation of small-displacement stiffness, E*py, with depth for varying e/Lp. φ_{tr} = 37°, E_s = 93 MPa, D = 2 m, wt = 0.05 m and L_p = 20 m.*

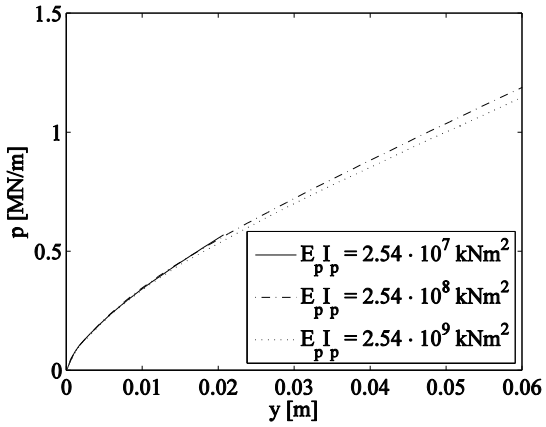

Figure 8 Comparison of p-y curves for varying pile bending stiffness. φ_{tr} = 40°, E_s = 74 MPa, D = 4 m, wt = 0.05 m, L_p = 20 m and e/L_p = 0.75.

4.2 Modified expression for the small-displacement stiffness of the p-y curves

Figure 4 and Figure 6 indicate that the small-displacement stiffness of the *p-y* curves, E^*_{py}, depends on the depth below the soil surface, *x*, Young's modulus of elasticity for the soil, E_s, and the pile diameter, *D*. A modified expression for the small-displacement stiffness is proposed in equation (7).

$$E^*_{py} = a\left(\frac{x}{x_{ref}}\right)^b \cdot \left(\frac{D}{D_{ref}}\right)^c \cdot \left(\frac{E_s}{E_{s,ref}}\right)^d \qquad (7)$$

b, *c*, and *d* are dimensionless constants whereas *a* is a constant specifying the small-displacement stiffness for $D = D_{ref}$ = 1 m, $x = x_{ref}$ = 1 m and $E_s = E_{s,ref}$ = 1 MPa. Further, *x* and *D* should both be inserted in meters and E_s in MPa. Values of *a*, *b*, *c* and *d* have been found to 1000 kPa, 0.3, 0.5 and 0.8, respectively. These compare reasonably well with the values, cf. Section 2, proposed by Kallehave et al. (2012) and Leth (2013).

The constants *a*, *c* and *d* have been determined based on least squares fitting. Due to the discontinuity of the small-displacement stiffness around the point of zero deflection, the constant *b* has been determined by visual fitting of equation (7) with the *FLAC*^{3D} simulations.

Figure 9 shows E^*_{py} normalized with respect to $(E_s/E_{s,ref})^{0.8}$ for varying values of Young's modulus of elasticity for the soil and *D* = 4 m. It can be observed that equation (7) provides a reasonable description of the dependency of the internal friction angle when using *d* = 0.8. Similar results have been obtained for *D* = 1-7. The linear variation of E^*_{py} with depth, *b* = 1, and the non-linear expression proposed be Lesny and Wiemann (2006), *b* = 0.6, overestimates E^*_{py} for large depths.

In Figure 10, a normalised E^*_{py} for an internal friction angle of 40°, E_s = 74 MPa, and varying pile diameters is presented as function of depth. A constant bending stiffness corresponding to a steel pile with a pile diameter of 4 m and a wall thickness of 0.05 m has been employed for all piles in order to isolate the effect of the diameter to equation (7) only. The proposed expression for E^*_{py}, produces a reasonable fit.

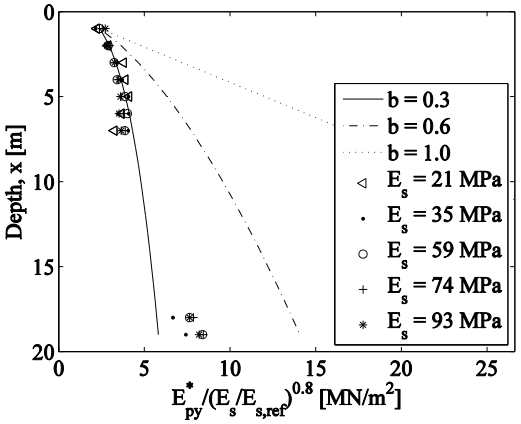

Figure 9 Normalized small displacement stiffness, E^*_{py}, for φ_{tr} = 37°, D = 4 m, wt = 0.05 m, L_p = 20 m and e/L_p = 0.75. The three curves have been forced through the average normalised small-displacement stiffness in a depth of 1 m.

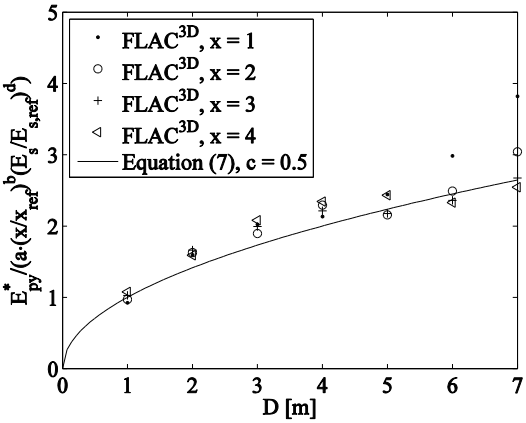

Figure 10 Normalised small-displacement stiffness for varying pile diameter and for φ_{tr} = 37°, E_s = 74 MPa, L_p = 20 m and e/L_p = 0.75. The bending stiffness has been kept constant for all piles.

4.3 Practical implications in relation to the modified expression for the small-displacement stiffness

When using equation (7) for determination of the initial slope of *p-y* curves for investigations of the serviceability limit state, the authors recommend employing an E_s corresponding to $E_{0.1}$, which is the Young's modulus of elasticity for an average axial strain of 0.1%, as monopiles used as foundation for offshore wind turbines are exposed to small deflections/rotations. According to Lunne et al. (1997), this level of strain is reasonably representative for many well-designed foundations.

5 EXAMPLE – HORNS REV 1

5.1 Description of Horns Rev 1 Offshore Wind Farm

The wind turbine considered in this example is a part of Horns Rev 1 Offshore Wind Farm, built during 2003 and located in the North Sea approximately 30 km west of Esbjerg in Denmark. The wind turbines at the site are all of the Vestas V80-2.0 MW type with a total assembly weight of 105.6 Te. The hub height is 70 m above MSL and the site is dominated by westerly winds. The foundations are monopiles having a diameter of 4.0 m. A transition piece with outer diameter of 4.34 m constitutes the transition from the tower to the monopile, cf. Hald et al. (2009).

5.2 Pile and loading conditions

The steel monopile considered is the foundation for wind turbine 14. The length is 31.6 m and the wall thickness, *wt*, and thereby the bending stiffness, E_pI_p, varies along the pile. The monopile has been driven to its final position 31.8 m below the mean sea level leading to an embedded length of 21.9 m.

The pile behaviour is investigated corresponding to the serviceability limit state (SLS): the horizontal load $H = 2.0$ MN and the overturning bending moment $M = 45$ MNm. More information on the pile geometry and the loading conditions can be found in Augustesen et al. (2010).

5.3 Soil conditions

The soil profile consists primarily of dense to very dense sand. The stratigraphy and the soil properties are presented in Augustesen et al. (2010).

For the *FLAC*^{3D} analyses the classical Mohr-Coulomb criterion and a linear elastic material model have been combined to describe the elasto-plastic material behaviour of the soil. Further details on the FLAC3D model of the wind turbine foundation are presented in Augustesen et al. (2010).

5.4 Results and discussion

In Figure 11, the calculated deflections are shown for the case in which the pile is subjected to the static SLS-loads. The pile behaviour has been determined by means of *FLAC*^{3D} and the Winkler model approach employing, respectively, the original API *p-y* curves given by equations (1)-(4) (in the following denoted the API method) and the API *p-y* curves employing the proposed small-strain stiffness given in equation (7) (in the following denoted the modified API method). The deflection patterns predicted by *FLAC*^{3D} and the modified API method have similar shapes. The monopile behaves relatively rigid implying that a "toe kick" occurs; this is especially pronounced when considering the deflection behaviour predicted by means of *FLAC*^{3D} and the modified API method. Below 14 m the deflection pattern estimated by the API method and *FLAC*^{3D} deviate significantly. *FLAC*^{3D} estimates, for example, greater horizontal deflections at the pile toe compared to the API method (Table 1). The deviation in deflection pattern may be due to the fact that the small-displacement stiffness, E^*_{py}, provided by the API method is overestimated at great depths. Since the API method overestimates the stiffness with depth compared to *FLAC*^{3D} and the modified API method, the depth for zero deflection predicted by the API method is located closer to the seabed (Table 1). Furthermore, the maximum horizontal deflection at seabed level determined by means of the API method is much lower compared to the deflections predicted by the other methods (Table 1).

The three approaches predict similar distributions of the moment with depth. Howev-

er, *FLAC*^{3D} estimates slightly lesser and higher moments at moderate and deep depths, respectively, compared to the API method and the modified API method. The maximum moments determined by the three approaches are almost identical (Table 1). The depths to the maximum moment vary between 2.5 m and 3.0 m with *FLAC*^{3D} giving rise to the smallest value.

The *p-y* curves at different depths are shown in Figure 12. Except for the depth $x = 2.1$ m the API method has a tendency to overestimate the soil resistance, *p*, at a given deflection, *y*, compared to the other two approaches. The pressures, estimated by means of *FLAC*^{3D}, mobilised at the depth $x = 7.4$ m are less than the pressures at both $x = 2.1$ m and $x = 3.9$ m for a given deflection *y*. This is due a the lower angle of internal friction and a lower Young's modulus of elasticity at that depth (Figure 12).

Generally, the modified API method predicts the results obtained by *FLAC*^{3D} better than the API method. The deviations, however, in the results determined by means of *FLAC*^{3D} and the modified API method may be caused by: the traditional uncertainties related to numerical modelling; shortcomings in the method proposed by Georgiadis (1983), in which layered soil profiles have been taken into account; shortcomings in the general shape of the *p-y* curves; and shortcomings in the definition of the ultimate soil resistance.

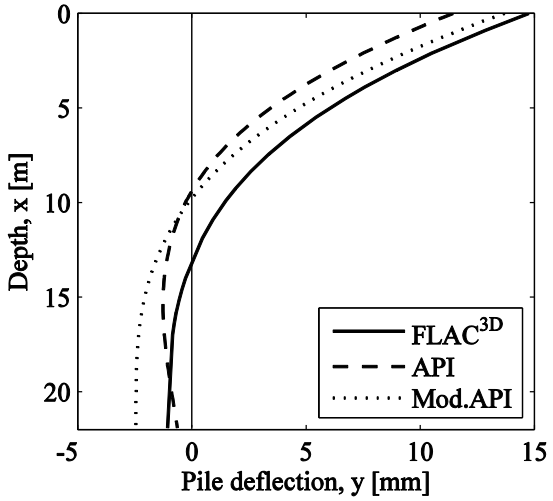

Figure 11 Pile deflection at maximum horizontal load for the monopile foundation of Wind Turbine 14 at Horns Rev 1.

Table 1 Distribution of bending moment, pile deflection and pile rotation.

	***FLAC*^{3D}**	**API**	**Mod. API**
Max moment [MNm]	47.1	48.8	48.3
Depth to max. moment [m]	2.5	3.0	2.8
Pile deflection, seabed [mm]	14.8	11.4	13.7
Pile deflection, toe [mm]	-1.0	-0.6	-2.5
Rotation, seabed [°]	0.12	0.12	0.13
Depth to zero deflection [m]	13.2	9.4	9.8

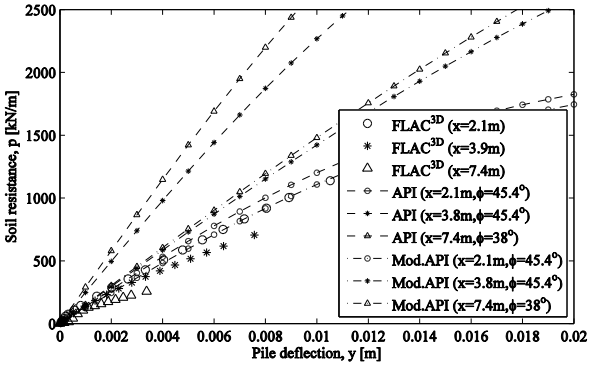

Figure 12 Soil resistance as a function of pile deflection and depth for Wind Turbine 14 at Horns Rev 1.

6 CONCLUSIONS

This paper considers large-diameter stiff monopiles in sand for offshore wind turbines. In design of such piles the first part of the *p-y* curves are especially important. A modified expression for the small-displacement stiffness of the *p-y* curves has been proposed, in which the slope depends on the depth below the soil surface, the pile diameter and Young's modulus of elasticity of the soil. This is in contrast to the method recommended by the American Petroleum Institute (API) in which the initial part of the *p-y* curves is independent of Young's modulus of elasticity and the diameter. The reassessment of the *p-y* curves recommended by the API is based on three-dimensional numerical analyses and the reassessment is aiming for a better prediction of the pile behaviour, especially when exposed to static SLS loads.

The differences in pile behaviour by employing a Winkler model incorporating the current *p-y* curves recommended by API and a modified version in which the expression for the small-displacement stiffness of the *p-y* curves proposed in this paper is employed, respectively, has been evaluated. The assessment is based on a monopile for an offshore wind turbine at Horns Rev, Denmark. A three-dimensional numerical model of the pile at Horns Rev has also been established by means of the commercial software package *FLAC*^{3D}. Generally, the modified API method predicts the results obtained by *FLAC*^{3D} considerably better than the API method.

7 REFERENCES

Achmus, M., Kuo, Y.-S. & Abdel-Rahman, K. (2009). Behavior of monopile foundations under cyclic lateral load. Comput. Geotech., Vol. 36, No. 5, 725-735.

ANSI/API (2011). Recommended Practice for Geotechnical and Foundation Design Considerations, API RP2GEO. American Petroleum Institute, 1. Edition.

Ashford, S.A. & Juirnarongrit, T. (2003). Evaluation of pile diameter effect on initial modulus of subgrade reaction. J. Geotech. Geoenv. Eng., Vol. 129, No. 3, 234-242.

Ashour, M. & Norris, G. (2000). Modeling lateral soil-pile response based on soil-pile interaction. J. Geotech. Geoenv. Eng., Vol. 126, No. 5, 420-428.

Augustesen A.H., Sørensen S. H. S., Ibsen L. B., Andersen L., Møller M. & Brødbæk K. T, 2010. Comparison of calculation approaches for monopiles for offshore wind turbines. In proceedings of Numerical Methods in Geotechnical Engineering 2010, Trondheim, Norway. Benz & Nordal (eds). Taylor & Francis Group. pp. 901-906

Bogard, D. & Matlock, H. (1980). Simplified Calculation of p-y Curves for Laterally Loaded Piles in Sand, Unpublished Report, The Earth Technology Corporation, Inc., Houston, Texas.

Brinkgreve, R.B.J. & Swolfs, W. (2007). PLAXIS 3D FOUNDATION, Material Models manual, Version 2. PLAXIS b.v.

Carter, D.P. (1984). A non-linear soil model for predicting lateral pile response. Civil Engineering Dept., Univ. of Auckland, New Zealand, Rep. No. 359.

Chik, Z.H., Abbas, J.M., Taha, M.R. & Shafiqu Q.S.M. (2009). Lateral behavior of single pile in cohesionless soil subjected to both vertical and horizontal loads. Eur. J. Sci. Res., Vol. 29, No. 2, 194-205.

Cox, W.R., Reese, L.C. & Grubbs B.R. (1974). Field testing of laterally loaded piles in sand. Proceedings of the Sixth Annual Offshore Technology Conference, Houston, Texas, USA, 459-464.

DNV (2014). Design of Offshore Wind Turbine Structures, DNV-OS-J101. Det Norske Veritas, Det Norske Veritas Classification A/S.

Fan, C.C. & Long, J.H. (2005). Assessment of existing methods for predicting soil response of laterally loaded piles in sand. Comput. Geotech., Vol. 32, 274-289.

FLAC^{3D} 3.1 manual (2006). Fast langrangian analysis of continua in 3 dimensions. Itasca Consulting Group Inc., Minneapolis, Minnesota, USA.

Georgiadis, M. (1983). Development of p-y curves for layered soils. In Proc. of the Conference on Geotechnical Practice in Offshore Engineering, 536–545.

Hald, T., Mørch, C., Jensen, L., Bakmar, C.L. & Ahle, K. (2009). Revisiting monopile design using p-y curves – Results from full scale measurements on Horns Rev. European Offshore Wind 2009, Stockholm, Sweden.

Ibsen, L.B., Hanson, M., Hjort, T.H. & Thaarup, M. (2009). MC parameter calibration for Baskarp Sand No. 15. DCE Technical Report No. 62, Department of Civil Engineering, Aalborg University, Denmark.

Kallehave, D., Thilsted, C. L. & Liingaard, M. A. 2012. Modification of the API p-y formulation of Initial Stiffness of Sand. In Proc. of Offshore Site Investigation and Geotechnics: Integrated Techologies – Present and Future, London, UK.

Kim, Y. & Jeong, S. (2011). Analysis of soil resistance on laterally loaded piles based on 3D soil-pile interaction. Comput. Geotech., Vol. 38, 248-257.

Kirsch, F., Richter, T. & Coronel, M. (2014). Geotechnische Aspekte bei der Gründungsbemessung von Offshore-Windenergieanlagen auf Monopfählen mit sehr grossen Durchmessern, Stahlbau.

Klinkvort, R.T., Leth, C.T. & Hededal, O. (2010). Centrifuge modelling of a laterally cyclic loaded pile. Proceedings of International Conference on Physical Modelling in Geotechnics, Zürich, Switzerland, 959-964.

Kramer, S.L. (1996). Geotechnical Earthquake Engineering. Prentice-Hall International Series in Civil Engineering and Engineering Mechanics, William J. Hall (eds.), ISBN0-13-374943-6.

Lengkeek, H.J. (2003). Estimation of sand stiffness parameters from cone resistance. PLAXIS Bulletin No. 13, 15–19.

Lesny, K. & Wiemann, J. (2006). Finite-element-modelling of large diameter monopiles for offshore wind energy converters, Geo Congress 2006, Atlanta, Georgia, USA.

Leth, C.T. (2013). Improved Design Basis for Laterally Loaded Large Diameter Pile: Eperimental Based Approach [Dissertation]. Department of Civil Engineering, The Faculty of Engineering and Science, Aalborg University, Aalborg, Denmark.

Ling, L. F. (1988). Back analysis of lateral load test on piles. Civil Engineering Dept., Univ. of Auckland, New Zealand, Rep. No. 460.

Lunne, T., Robertson, P.K. & Powell J.J.M. (1997). Cone penetration testing in geotechnical practice. Blackie Academic & Professional.

Murchison, J.M. & O'Neill, M.W. (1984). Evaluation of p-y relationships in cohesionless soils. Analysis and design of pile foundations. Proceedings of a Symposium in conjunction with the ASCE National Convention, New York, New York, USA, 174-191.

Sørensen S. P. H., Ibsen L. B. & Foglia A., 2015. Testing of Laterally Loaded Rigid Piles with Applied Overburden pressure. International Journal of Offshore and Polar Engineering, Vol. 25, No. 2, June 2015, pp. 120-126.

Terzaghi, K. (1955). Evaluation of coefficients of subgrade reaction, Geotech., Vol. 5, No. 4, 297-326.